

Study of the temperature effect on the functioning of photodetecting lighting elements and calculation of their reliability

Vasyl Martsenyuk^{1,2,*†}, Andrii Sverstiuk^{2,3,†}, Taras Dubyniak^{2,†}, Petro Mykulyk^{2,†},
Nadia Shostakivska^{2,†} and Mykola Poshyvak^{2,†}

¹ University of Bielsko-Biala, Willowa St. 2, Bielsko-Biala, 43-300, Poland

² Ternopil National Ivan Puluj Technical University, Rus'ka str. 56, Ternopil, 46001, Ukraine

³ I. Horbachevsky Ternopil National Medical University, Maidan Voli, 1, Ternopil, 46002, Ukraine

Abstract

The article deals with the design and development of an adaptive lighting system. This task is relevant, since with the development of technology, there is a problem in automating lighting systems to save electricity consumption. According to statistics, about 40% of the generated electricity is consumed for lighting. One of the main benefits of an adaptive lighting system is its ability to provide tremendous energy savings. This can be achieved by giving lighting devices a certain degree of autonomy. A well-functioning adaptive lighting system can be much more efficient than one that relies solely on human decisions. In order for a lighting system to make autonomous decisions about light emission and operation, it must be provided with a stream of information on which to base those decisions. Most of this data comes from sensors. A sensor-driven network of smart bulbs is able to monitor changes in the environment and interpret those changes to dynamically adjust its operation for optimal comfort and energy efficiency, and to reduce energy bills.

Keywords

mathematical support, photodetector, LED, error, metrological analysis, inaccurate value

1. Introduction


To solve the problems of controlling and managing lighting, we used the occupancy sensing method, which is implemented through the use of presence sensors and allows you to automatically dim or turn on or off the light after a certain space has been free for a certain period of time specified by the user. The problems of the measurement process and accuracy are described in a number of works by well-known scientists of Ukraine and foreign authors

ICyberPhyS-2024: 1st International Workshop on Intelligent & CyberPhysical Systems, June 28, 2024, Khmelnytskyi, Ukraine

* Corresponding author.

† These authors contributed equally.

✉ vmartsenyuk@ath.bielsko.pl (V. Martsenyuk); sverstyuk@tdmu.edu.ua (A. Sverstiuk); d_taras@ukr.net (T. Dubyniak); mykpet7@gmail.com (P. Mykulyk); Shostakivska@ukr.net (N. Shostakivska); claruspauer01@gmail.com (M. Poshyvak)

 0000-0001-5622-1038 (V. Martsenyuk); 0000-0001-8644-0776 (A. Sverstiuk); 0000-0003-1529-6951 (T. Dubyniak); 0000-0001-6008-6510 (P. Mykulyk); 0000-0002-7732-6186 (N. Shostakivsk); 0009-0009-9655-4123 (M. Poshyvak);



© 2023 Copyright for this paper by its authors. Use permitted under Creative Commons License Attribution 4.0 International (CC BY 4.0).

such as Arshan E.V., Bondarenko R.I., Kalachnikov O.O., Sidnev O.B., Semikina T.V. [2], [3], [4]. It is also reflected in the works of other authors [5], [6].

2. Problem statement

2.1. Features of the functioning of photocouplers for domestic premises (single-phase switching)

Occupancy sensing is one of the most common lighting control methods used in modern buildings. Simply put, it allows you to automatically dim or turn off the lights after no movement and/or human presence is detected in a certain space for a certain period of time, defined by the user, zone 1.

As soon as motion is detected, the lighting is turned on again or dimmed according to the set scenarios. Motion detection is performed by motion sensors using infrared, ultrasonic, or microwave sensing technology.

The number of sensors that should be placed in a given space to provide the lighting system with correct data depends on both the size and type of the space and the desired lighting performance in it. A simpler scenario involves all the bulbs working in sync and providing the same level of light intensity throughout the space as long as the occupant is in view of any of the installed sensors. A somewhat more complex scenario that provides more efficient operation is to divide the space into several separate lighting zones, each of which is associated with one or more sensors. Each time motion is detected in one of the zones, the lighting of only that particular zone 2 is turned on. This division into zones (an example is shown in fig. 1) is especially effective in large open spaces, staircases, or long corridors.

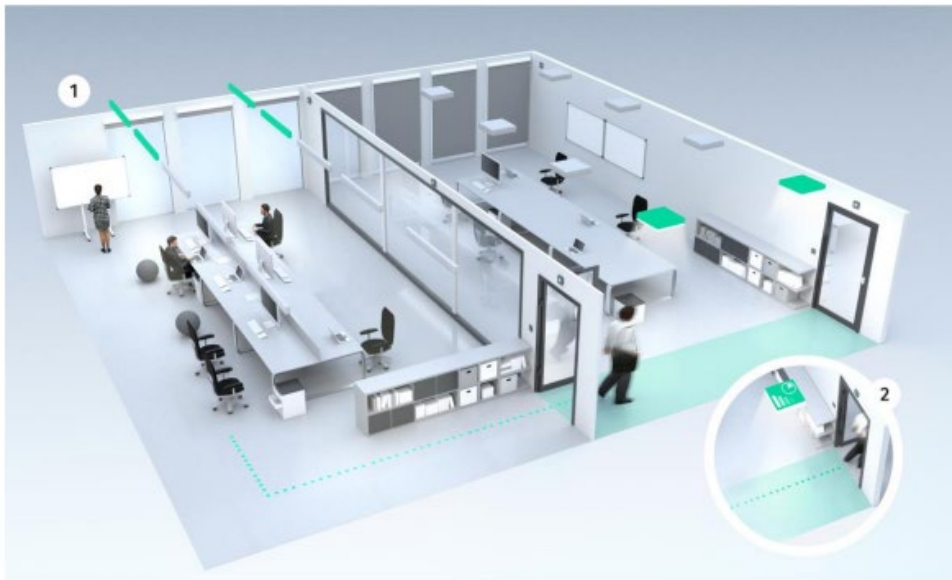


Figure 1: Dividing the room into lighting zones.

If you look at the room on the right (see Figure 1), you will notice that only a part of it is lit. This is because the person entering the room only walks through it to get to another room, so

there is no need to turn on all the lights in that room. In this case, only some of the lights are activated, and as soon as the person leaves the room, the lights turn off. Without dividing the space into zones and matching local lighting with motion sensors, the entire space would remain fully illuminated all the time, resulting in higher energy costs. Implementation experience and calculations confirm the effectiveness of occupancy sensing in office spaces in terms of energy efficiency. The most efficient scenario in terms of energy efficiency is when motion sensors are built directly into the lighting fixtures. This allows each device to respond autonomously to signals from the sensor installed in it. This approach is effective for office spaces or certain types of manufacturing plants, as each workstation is treated as a separate zone that is only illuminated when the employee is present at their workstation. Occupancy sensing is a proven strategy for reducing energy consumption and lighting costs.

For this reason, sensing is often a requirement of commercial building energy codes [3]. The potential savings offered by such a system depend heavily on the types of spaces, with the greatest benefits being realized in those where employees work intermittently, such as classrooms or offices. However, an overall reduction in light load of approximately 20-30% can be achieved in most commercial environments. The concept of occupancy sensing is virtually the same for both wired and wireless lighting control systems. Wireless solutions provide the flexibility to install an adaptive sensor lighting system. The use of wireless technologies significantly reduces the time required to install a sensor network and reduces the labor intensity of the lighting system installation process. Another advantage is that there is no need to physically lay cables. And the problem of power supply to the sensors is effectively solved using Bluetooth Smart wireless connection technology [4]. Thanks to the support of the "sleep nodes" protocol, which spend most of their time in standby mode and wake up only when prompted by an ID call to perform their task, and then go back to sleep, such an intelligent wireless lighting system can operate for years without replacing batteries.

Adaptive lighting control systems can be divided into two types: local and general lighting control systems. Local lighting is used for work areas and workspaces, i.e. places where more lighting is required. Such systems can be simplified, as they are responsible for only one or a few light sources. The development and installation of an adaptive local lighting system is a relevant task if the workplace is used periodically. Such a system can be built using a light (or presence) sensor and a data processing module (fig. 2).

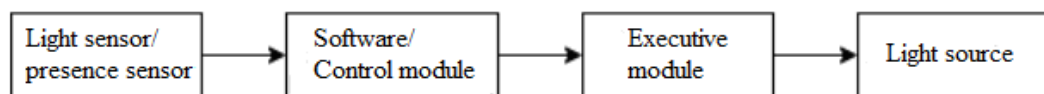


Figure 2: Block diagram of a local lighting control system.

It is advisable to organize communication between the system modules using a wired connection. Such a connection can be organized using the RS-485 standard or a UTP5 cable. Since the modules of such a system are located at a short distance from each other, such a connection will provide a relatively higher system speed and fewer errors in signal transmission. The disadvantage of such a connection is the design aspects that require wiring during installation.

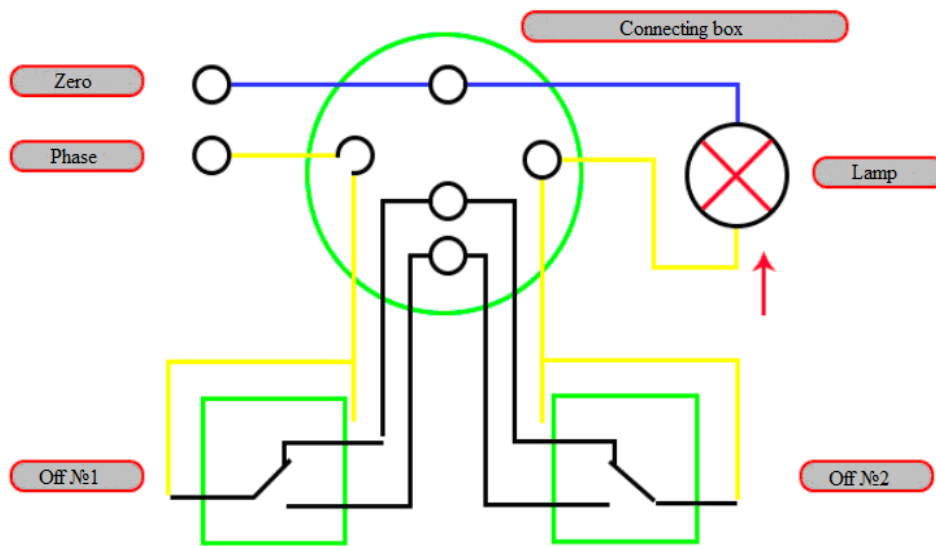


Figure 3: Electrical circuit diagram for domestic premises.

2.2. Features of the functioning of photodetecting elements for (three-phase) switching

Figure 4 shows the electrical structural diagram of the ROP-15-16-24 dimmer.

The lighting of the territories of agricultural enterprises at night is switched on automatically with the help of various devices, including: photo relays, photo switches. [5]

The FM photorelay is designed to automatically switch street lighting on and off depending on natural light. Fig. 5 shows the electrical circuit diagram of the FR-2 photorelay.

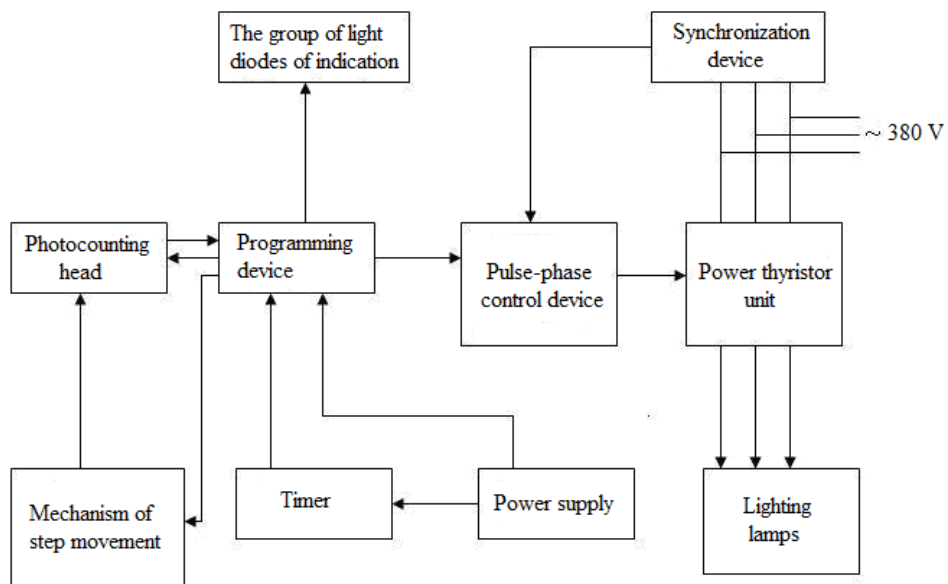


Figure 4: Electrical structure diagram of the dimmer.

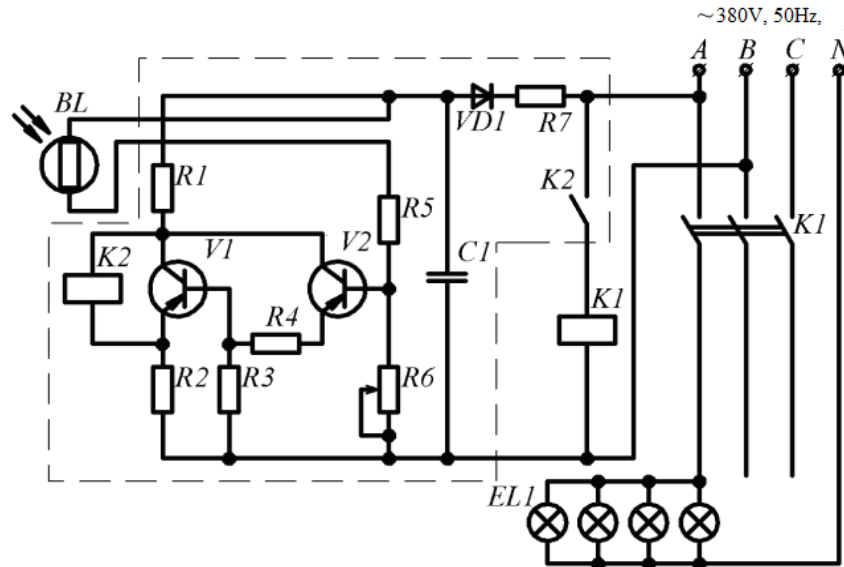


Figure 5: Electrical circuit diagram of street lighting control with the help of FR-2 photorelay.

A hermetically sealed photo resistor of the FSK-GI type is used as a photodetector of the FR-2 photo relay. The photo resistor can be mounted in the device body or, depending on the operating conditions, can be placed separately from the relay. The photo resistor should be installed so that its surface is not exposed to direct sunlight. The principle of operation of the photo resistor is as follows:

Increasing the illumination reduces the resistance of the photo sensor. This changes the potential on the base of the transistor VT2. The transistor VT2 opens and opens the transistor VTI, which shunts the relay winding K2. This leads to the disconnection of the magnetic starter K1.

When the illumination decreases, the photo sensor resistance increases, the transistors VT1 and VT2 close, the relay K2 is triggered, and the magnetic starter turns on. The circuit is adjusted by changing the resistance R6. The manufacturer manufactures the photo relay set to turn on street lighting at 5 lux and turn it off at 10 lux.

For automatic switching on and off of street lighting, the FV-2 photo control switch is widely used, which is designed to automatically switch street lighting on and off depending on the level of natural light. Technical data of the FV-2 photo switch:

- load switching on at illumination, lux 1.3 ± 1
- load switching off at illumination, lux 7 ± 2
- long-term permissible current, A 20A

The operation of the photo switch is based on the principle of changing the resistance of the photo sensor BL depending on the illumination. The photo resistor FSK-G2 is used as a sensor.

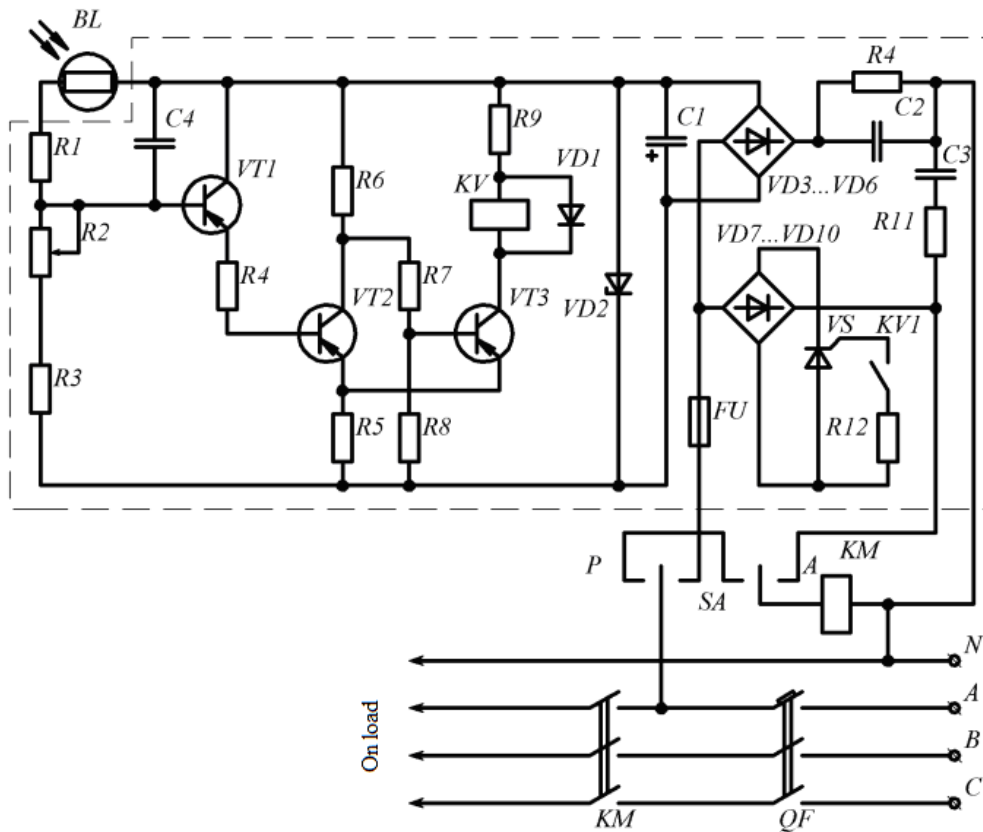


Figure 6: Electrical schematic diagram of the FV-2 photo switch.

The electrical circuit of the photo switch (fig. 6) consists of a Schmitt trigger circuit breaker on transistors VT1, VT2, VT3, a bridge thyristor key on the rectifier block VD7-VD10, a thyristor VS, and a magnetic starter KM. The thyristor key is controlled by the contacts of the KV relay.

When the illumination increases to 7 ± 2 lux, the resistance of the photo sensor decreases, a negative bias is applied to the base of the transistor VT1, the transistor VT1 opens, causing an increase in the negative voltage on the base of the transistor VT2, which begins to open. The negative voltage across transistor VT3 decreases, and transistor VT3 begins to close. The negative feedback voltage across the resistor R5 decreases, which contributes to the development of an avalanche-like process, as a result of which the transistor VT2 goes into saturation mode, and the transistor VT3 closes. The relay KV remains powered, the thyristor VS closes, and the magnetic starter KM turns off the lighting load.

When the illumination decreases to 1.3 ± 1 lux, the resistance of the photo sensor increases, the negative offset on the base of the transistor VTI decreases, and the transistor closes, which leads to a decrease in the negative voltage on the base of the transistor VT2. The transistor VT2 begins to close. The negative voltage on the base of transistor VT3 increases. The transistor VT3 starts to open. The negative feedback voltage across the resistor R5 increases, which contributes to the development of an avalanche-like process, as a result of which the transistor VT2 closes and the transistor VT3 goes into saturation

mode. When the transistor VT3 is open, the relay KV is triggered, the thyristor VS opens, and the magnetic starter KM turns on the lighting load. The range of operation of the circuit is regulated by the resistor R2. The SA operating mode switch has three positions: "ON", "0", "AUTO" [5].

3. Calculating the reliability of the designed product

Reliability is the ability of a device (element or system) to perform its intended functions. Reliability is determined by the reliability of operation and maintainability.

Since failures and recovery are random events in the sense that the place and time of their occurrence cannot be predicted precisely, reliability is quantified by probabilistic characteristics.

The probability of failure-free operation (PFO) of an element $p(t)$ or a system $p_c(t)$ is the probability that no failure will occur within a given operating time t under specified operating conditions.

Failure intensity $\lambda(t)$ is the conditional probability density of device failures, determined for a certain moment in time, provided that no failures have occurred up to that moment [6].

The relationship between the failure rate and the probability of failure-free operation can be obtained as follows:

$$p(t) = \exp \left[- \int_0^t \lambda(t) dt \right] \quad (1)$$

Reliability against sudden operational failures ($\lambda_0 = \text{const}$) is calculated for the period of normal operation, when the initial service life (entering modes) has already expired, and failures due to wear and ageing have not yet occurred. For complex equipment of various types, the failure rate of the system can be considered constant also in the wear area.

The calculation is based on the principle of determining system reliability indicators by the reliability characteristics of component parts, which makes it possible to carry out the calculation in the process of designing equipment consisting of known elements and components. To do this, it is necessary to clarify the above expressions for the reliability indicators of elements $p(t)$, $q(t)$, $\omega(T)$, TCP , T_0 , taking into account the constancy of the failure rate [7].

The formula for the probability of uptime takes the form:

$$p(t) = \exp \left[- \int_0^t \lambda(t) dt \right] = \exp(-\lambda_0 t) \quad (2)$$

This relationship is known as the exponential law of reliability. The argument t does not mean calendar time, but the interval for which reliability is calculated. For the assumption $\lambda_0 = \text{const}$, the probability of failure for the same time interval t does not depend on how the starting point of this interval is chosen [8].

The mean time between failures can then be found:

$$T_{CP} = \int_0^{\infty} p(t)dt = \int_0^{\infty} \exp(-\lambda_0 t) dt = \frac{1}{\lambda_0} \quad (3)$$

By grouping equally reliable elements, we get the following:

$$p_c(t) = \exp\left(-t \sum_{j=1}^m \lambda_{0j} N_j\right) \quad (4)$$

where λ_{0j} is the failure rate of the j -th group;
 N_j is the number of elements of the j -th group;
 m is the number of groups of equally reliable elements.
 Failure rate of the device as a whole:

$$\lambda_c = \sum_{j=1}^m \lambda_{0j} N_j \quad (5)$$

An approximate calculation of reliability is performed at the technical design stage using the above formulas. The values of the λ -characteristics (failure rate) of the device elements are determined from the reference data [9].

When calculating the reliability, the influence of operating conditions, temperature and electrical mode is taken into account using the following ratios:

$$p_c(t) = \exp\left(-k_\lambda \sum_{j=1}^m \lambda_j N_j\right) \quad (6)$$

$$\lambda_c = k_\lambda \sum_{j=1}^m \lambda_j N_j \quad (7)$$

$$\lambda_j = \lambda_{0j} \alpha_j \quad (8)$$

$$k_\lambda = k_{\lambda 1} k_{\lambda 2} k_{\lambda 3} \quad (9)$$

where λ_j is the failure rate of the j -th equally reliable group of elements during operation under specified conditions;

λ_{0j} - the same, but when operating in nominal mode;

α_j is the correction factor for the failure rate of the j -th group, which takes into account the influence of ambient temperature and the electrical load of the element.

The correction factor k_λ takes into account the operating conditions of the RAS; $k_{\lambda 1}$ - the influence of mechanical factors (vibrations, shock loads), $k_{\lambda 2}$ - the influence of climatic factors (temperature, humidity), $k_{\lambda 3}$ - operating conditions at low atmospheric pressure.

The values of the correction factor α depending on the temperature and load factor k_H , as well as the failure rate of the device elements, are taken from reference tables [10]. In this case, the load factor is defined as the ratio of the load for a certain parameter (power, current, voltage) acting on the element to its rated load, which is established by regulatory and technical documentation:

Power load factor:

$$K_p = \frac{P_p}{P_H} \quad (10)$$

where P_P is the operating value of the scattering power;
 P_H is the nominal value of the dissipation power.
Load factor by voltage:

$$K = \frac{U_P}{U_H} \quad (11)$$

where U_P is the operating voltage value;
 U_H is the nominal voltage value.

When designing, the electrical load factor is usually taken to be 0.4...0.8.

The temperature and load factor can be determined experimentally (at the stage of testing the prototype) or by calculation. Typical values of correction factors are also taken from the reference literature [11].

The following data is required to calculate the reliability of a radio device:

- a list of components (elements);
- the number of elements of each type;
- operating conditions;
- reference data on the intensity of ERE failures.

Reliability is calculated in the following sequence:

1. Draw up a table of input data for the calculation, determine the design characteristics of the components (for example, for transistors - silicon or germanium, or field effect, for capacitors - electrolytic or ceramic, etc.), determine the number of elements by groups for which to determine the values of the correction factors α_i , the value of the failure rate λ_0 from the table [12]. Calculate the failure rate λ_i for each group of components.
2. To take into account the operating conditions, determine the correction factors from the tables according to the operating conditions of the designed radio device and calculate the total coefficient K_λ . If the operating conditions correspond to laboratory conditions, K_λ is assumed to be 1.
3. Calculate the failure rate.
4. Calculate the average operating time before failure in accordance with the formula and taking into account.
5. Calculate the probability of failure of the radio device for the given values of time t_p . It is recommended to choose the number of values of t_p in the range of 6 - 10.
6. Based on the results of the calculations, plot the dependence of the probability of failure of the radio device on time t_p . Calculating the reliability of the REA.

The calculation of the reliability of the REA is significantly reduced when using the NAD_Release computer program.

For the calculation to be effective, the following requirements are imposed on the program.

Calculation of the probability of failure-free operation and the average operating time before failure of electronic equipment, taking into account the operating conditions.

Saving the calculation results as a file with the ability to print, as well as with the ability to further process the results in other programs (for example, in MatchCAD).

Visualization of the calculation results in the form of a graph of the dependence of the probability of failure on the device's operating time.

Availability of a computer database of failure rates of various electronics and electromechanical units of the RPS.

The ability to edit the database to take into account the characteristics of different devices.

Possibility to update the database with the characteristics of new items;

Possibility to correct data on the failure rate and other operational characteristics of radio elements during the calculation process;

Convenient and clear user interface of the program.

The program window is shown in Figure 7.

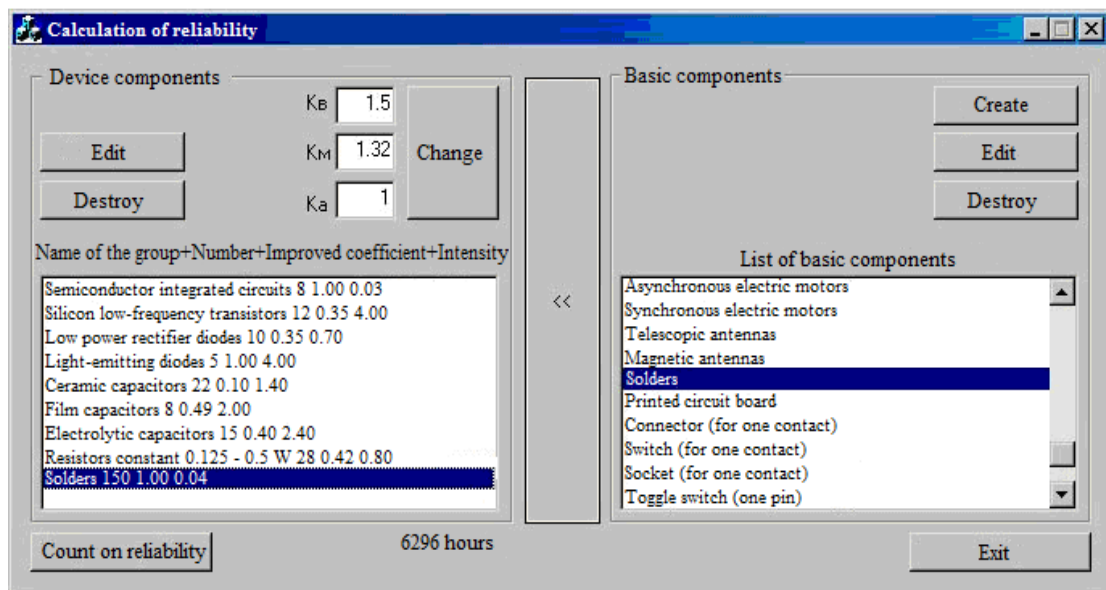


Figure 7: Main window of the reliability calculation program.

The results are output to a file:

- input data table (list of device components - name of the component group, number of elements in the group, failure rate, correction factor, total failure rate for this type of element);
- values of the influence coefficients $k\lambda_1$, $k\lambda_2$, $k\lambda_3$;
- the total failure rate of the device;
- average time between failures;
- data for plotting the dependence of the probability of failure on the service life.

4. Results and discussion

The following results were obtained as a result of the calculation: Calculation of the reliability of the designed laboratory power supply [13]. Reliability calculation. The initial data for reliability calculation are presented in Table 1.

Table 1
Initial data for reliability calculation

n/a	Name of the element group	Quantity pcs.	Kfact	Ividm*1e-06	Quantity*Knaf from*1e-06
1	Semiconductor integrated circuits	5	1	0.03	0.15
2	Transistors of low-frequency silicon	5	0.35	4	7
3	Low power rectifier diodes	9	0.35	0.7	2.205
4	LEDs	1	1	4	4
5	Ceramic capacitors	6	0.1	1.4	0.84
6	Electrolytic capacitors	8	0.4	2.4	7.68
7	Resistors 0.125 - 0.5 W constant	16	0.42	0,8	5.376
8	Power transformers	1	0.1	3	0.3
9	Throttles	1	0.1	1	0.1
10	Incandescent light bulbs	1	1	1.2	1.2
11	Printed circuit board	3	1	0,1	0.1
12	Rations	155	1	0,02	3.1
13	Fuse	1	1	0,5	0,5

Influence factors:

- Mechanical impact coefficient: 1
- Coefficient of influence of humidity and temperature: 1
- Atmospheric influence coefficient: 1

Calculation results:

- Failure rate: 3.2551e-005 1/h
- Average time between failures: 30721.0 hours.
- Calculation of the probability of failure P(t):
- t = 10 hours. P(t) = 0.999675
- t = 100 hours. P(t) = 0.996750
- t = 1000 hours. P(t) = 0.967973
- t = 10000 hours. P(t) = 0.722159
- t = 100000 hours. P(t) = 0.038577

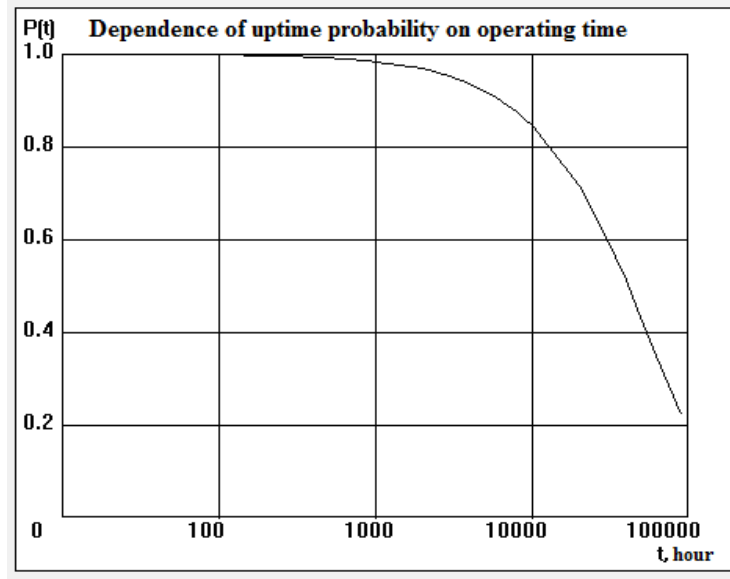


Figure 8: Graph of the dependence of $P = f(t)$.

When calculating the reliability of the device, all elements were calculated, taking into account the coefficients of mechanical stress, humidity and temperature, and the average time to failure was calculated to be 30721.0 hours [14].

Development of a mathematical model of the research object. Features of the functioning of photoreceiving elements. When designing a device, the choice of a contactless switch operating in the infrared spectrum is justified by the characteristics of the input signal.

The peak wavelength of infrared radiation of the human body at a temperature of 37°C is about 10 microns [15].

In this case, infrared radiation is characterized by less scattering in the working environment, which ensures better transmission through various media. The signal can be perceived within 1-8 cm from the detector.

Typical examples of infrared transmission media are vacuum, atmosphere, and optical fibers. In the atmosphere, absorption by H₂O, CO₂ and other components occurs at certain wavelengths [16].

Moreover, for certain frequency bands, the absorption intensity is lower, These include frequency bands from 3 microns to 5 microns and from 8 microns to 12 microns. These are sometimes referred to as "atmospheric windows" and are often used for non-contact control signal transmission.

To adjust the brightness, hold your hand in the switch area for 2 seconds until the desired light level is reached [17].

Compared to visible and ultraviolet rays, infrared radiation has a low energy, namely 1.24 eV at a wavelength of 1 micron and 0.12 eV at 10 microns. The energy of infrared radiation is expressed by the following equation:

$$E = hc/\lambda = 1.24/\lambda, \text{ eV}, \quad (12)$$

where $h \approx 4.14 \cdot 10^{-15}$ J is the Planck constant; $c \approx 3 \cdot 10^{10}$ cm/s is the speed of light;

λ is the wavelength in microns.

To increase the effectiveness of infrared radiation, the indicator should be cooled.

The main characteristics that indicate the efficiency of an infrared detector are the ratio of useful irradiation power to noise power [18].

Sometimes noise can also occur as a result of the impact of infrared radiation itself on the equipment. Their sources can be the infrared detector itself, its electrical circuit, or background fluctuations.

The photosensitivity is the ratio of the output voltage (or output current) to the number of watts of incident energy when noise can be neglected.

If the first two sources are ignored in comparison to the noise caused by background fluctuations, the ability of the device to respond to the control input is determined only by the noise from background fluctuations. This assessment is called "Background Limited Infrared Photo detection (BLIP)" [19].

5. Experimental part

Modelling the photodetector response to irradiation. The modelling was carried out in the MicroCap-8 system according to the connection scheme of the investigated element X1 shown in fig. 9. The parameters for describing the photocell (sensitivity, p-n junction capacitance, etc.) are set in its model. The effect of irradiation is simulated by a pulsed source Vlight. The output response is the voltage VOUT [20].

The analysis of the circuit in the frequency mode (Fig. 9) shows that the element responds stably to irradiation from the low-frequency region of the spectrum.

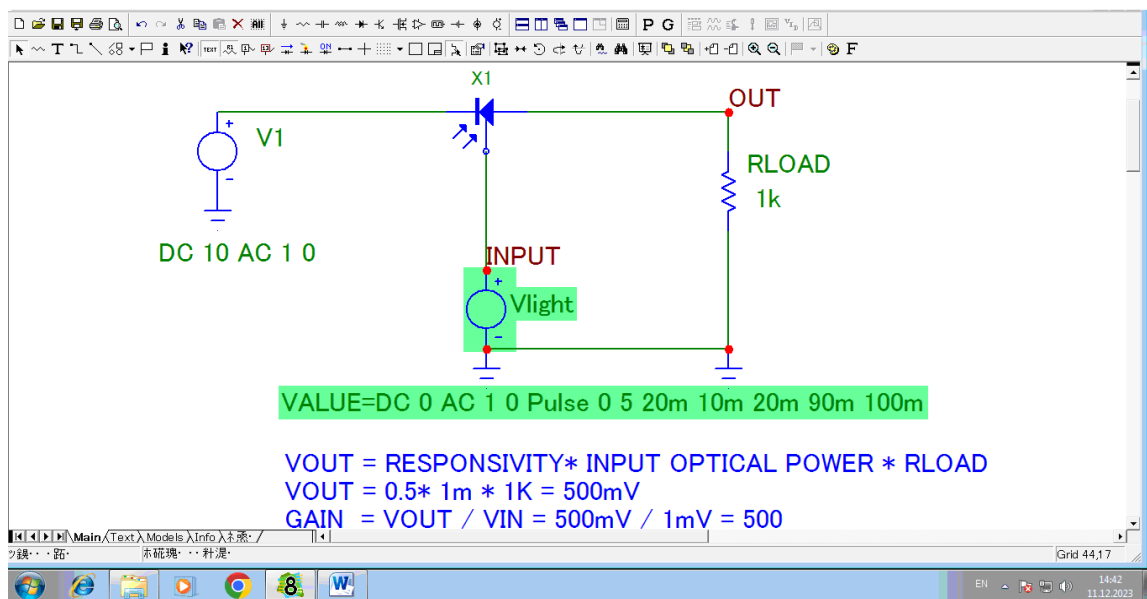


Figure 9: Scheme for studying the response of a photodiode element to irradiation.

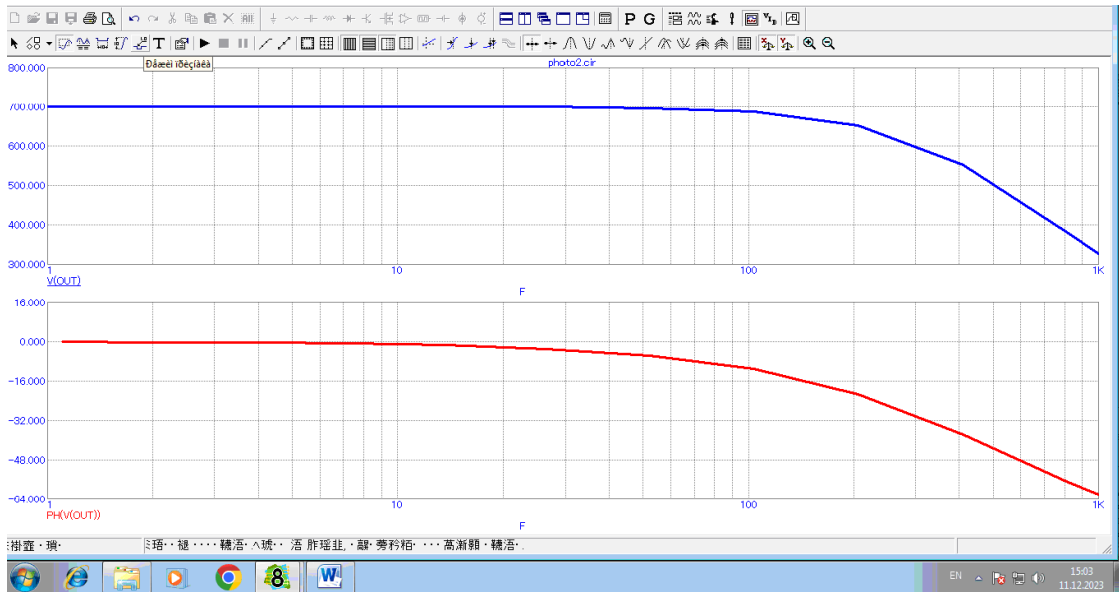


Figure 10: Frequency characteristics of the investigated photodiode element (upper graph - frequency response, lower graph frequency response).

Figs. 10, 11 show the results of the AC analysis: the response of the photodiode element to noise (Fig. 10) and control (Fig. 11) irradiation [21].

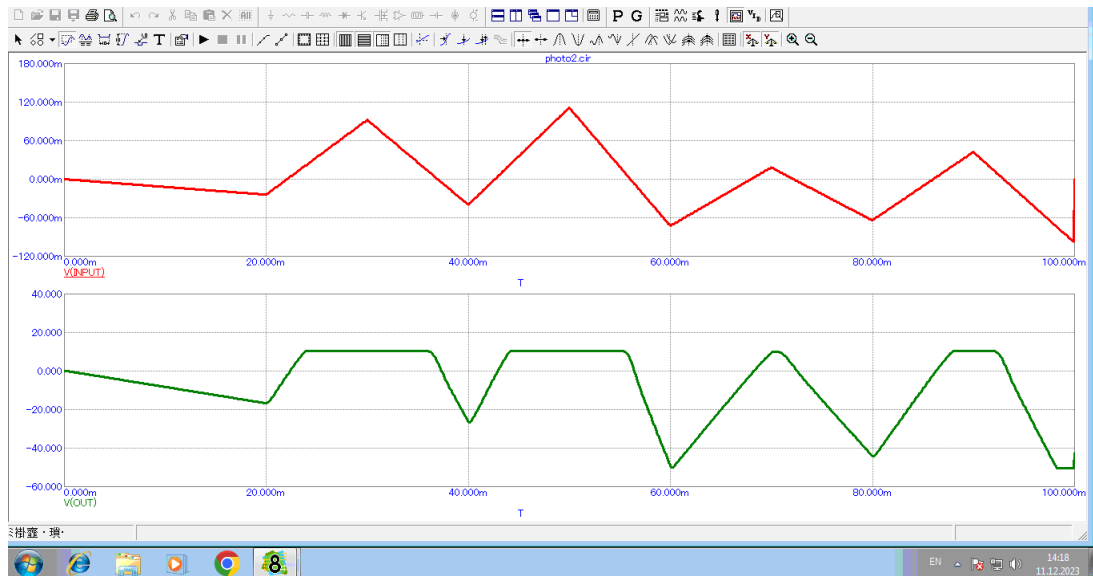
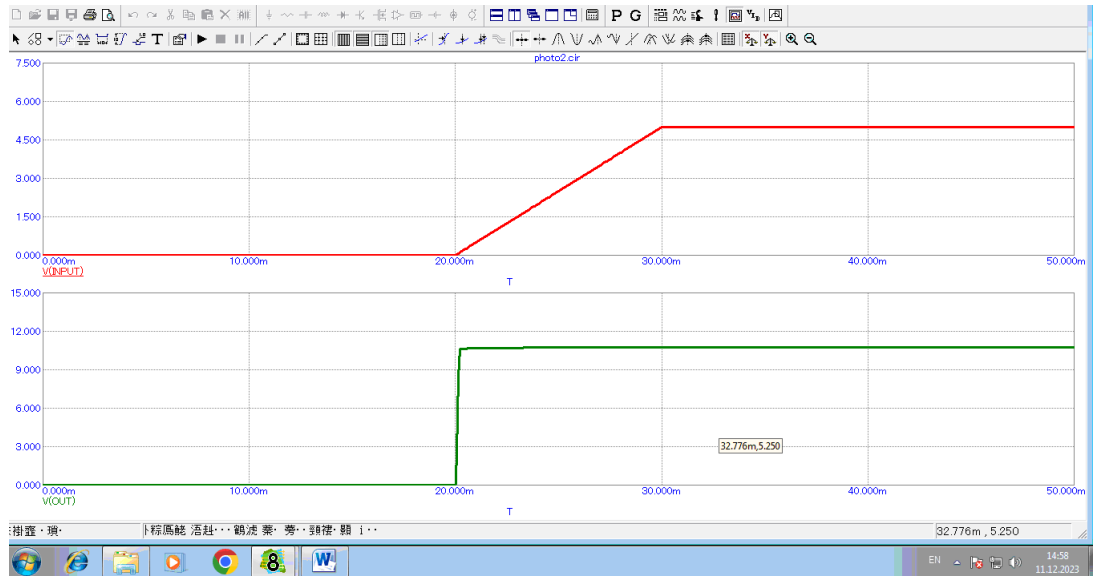
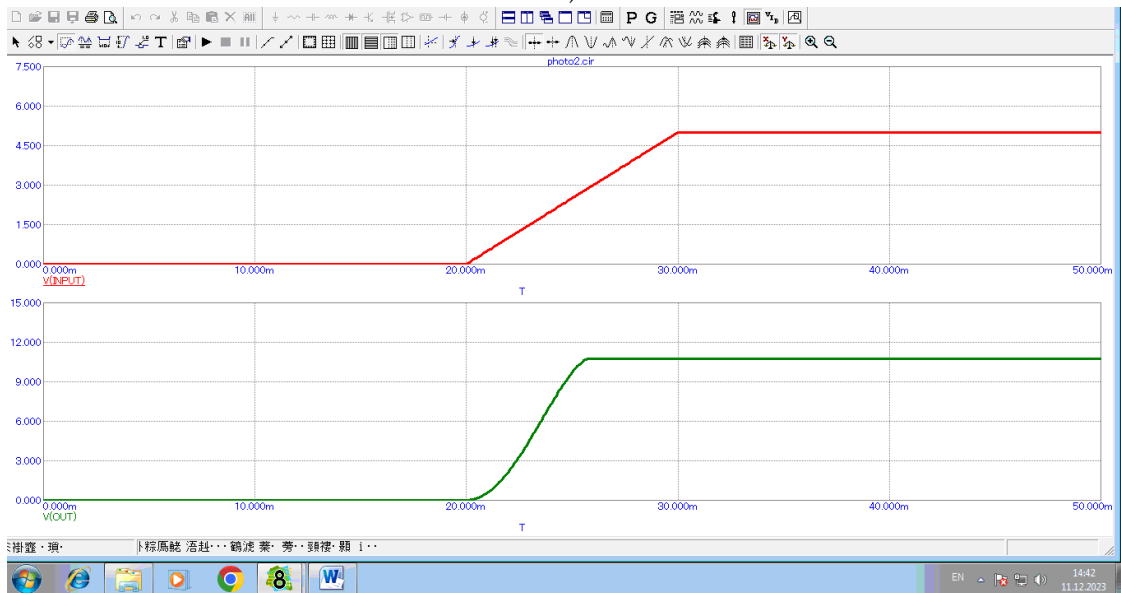


Figure 11: Response of a photodiode element to a low-frequency noise signal (upper graph - input signal, lower graph - load voltage).

In particular, in Fig. 12 a), b), we can see how photocells with different physical parameters (sensitivity and p - n junction capacitance) respond to the same control signal [22].



a)



b)

Figure 12: The response of photodiode elements of different brands (with different values of p-n junction capacitances) to the control signal (upper graph - input signal, lower graph - load voltage).

It should be noted that the dependences in Figs. 11, 12 were obtained in parallel at three values of the ambient temperature - 10°C, 20°C, and 30 °C, (deg. Celsius) [23], [24]. A promising direction is using the obtained results in cyber-physical systems [25].

As you can see, the photodetector's response to irradiation has not changed in this range (the graphs are superimposed).

6. Conclusion

Based on the calculations, it can be concluded that the contactless method is a constructive solution for domestic conditions. It is used to control lighting in rooms where it is important to avoid contact with foreign objects: in medical offices, kitchens, etc. It is best to use it at room temperature and away from direct sunlight.

When operating the designed device, it is recommended to use it in the temperature range from -20°C to $+50^{\circ}\text{C}$ degrees Celsius (instability may occur at very high or low temperatures). Reliable and protected devices should be used to control lighting in industrial premises.

References

- [1] M. Á. José Prieto, F. Nuño García, J. A. Martín Ramos, P. J. Villegas Saiz, R. Muñiz Sánchez, J. Díaz. Digital controllers for electrical engineering (microcontrollers, DSP, FPGA): main peripherals. 2023. In Encyclopedia of Electrical and Electronic Power Engineering. pp. 70–91. Elsevier. doi:10.1016/b978-0-12-821204-2.00011-8.
- [2] J. Sun. Design and research of wireless optical power meter based on IoT big data and physical quantity. In Results in Physics. 2023. Vol. 54, p. 107045. Elsevier BV. doi:10.1016/j.rinp.2023.107045.
- [3] J. An, et al., Load characteristics and impacts of different electric heating equipment integrated into power grid, In: 2019 IEEE 3rd Conference on Energy Internet and Energy System Integration. EI2, IEEE, pp. 1252-1257.
- [4] K. Berg, M. Resch, T. Weniger, S. Simonsen, Economic evaluation of operation strategies for battery systems in football stadiums, A Norwegian case study. J. Energy Storage 34, 102190. 2021.
- [5] Y. Song, H. Zhu, Y. Shen, Y. Deng, S. Feng. Multi-dimensional tunnel lighting environment model: Determining illuminance with regression analysis and parametric study on key factors. In Tunnelling and Underground Space Technology 2024. Vol. 151, p. 105864. Elsevier BV. doi:10.1016/j.tust.2024.105864.
- [6] A. E. Onile, E. Petlenkov, Y. Levron, J. Belikov. Smartgrid-based hybrid digital twins framework for demand side recommendation service provision in distributed power systems. In Future Generation Computer Systems. 2024. Vol. 156, pp. 142–156. Elsevier BV. doi:10.1016/j.future.2024.03.018
- [7] R. Ahshan, R. Al-Abri, H. Al-Zakwani, N. Ambu-Saidi, Solar PV system design for a sports stadium. In: 2019 IEEE 10th GCC Conference & Exhibition. IEEE, 2019, pp. 1-6.
- [8] S. A. Wagan, J. Koo, I. F. Siddiqui, M. Attique, D. R. Shin, N. M. F. Qureshi Internet of medical things and trending converged technologies: A comprehensive review on real-time applications. In Journal of King Saud University - Computer and Information Sciences. 2022. Vol. 34, Issue 10, pp. 9228–9251. Elsevier BV. doi:10.1016/j.jksuci.2022.09.005
- [9] M. Rouse, Smart home or building (home automation or domotics), TechTarget, 2020, <https://internetofthingsagenda.techtarget.com/definition/smart-home-or-building>.
- [10] B.-C. Zhao, W. Fan. High-luminance one-dimensional integral imaging display based on gradient-width line light sources. In Heliyon. 2024. Vol. 10, Issue 12, p. e32665. Elsevier BV. doi:10.1016/j.heliyon.2024.e32665.

- [11] D. Duraccio, P. P. Capra, G. Malucelli. UV-curable coatings for energy harvesting applications: Current state-of-the-art and future perspectives. In *Micro and Nano Engineering*. 2024. Vol. 23, p. 100266. Elsevier BV. <https://doi.org/10.1016/j.mne.2024.100266>.
- [12] *Data-Acquisition-Handbook, A Reference For DAQ and Analog & Digital Signal Conditioning*, 2012, MA, USA: Measurement Computing Corporation, 2023. URL: <http://www.mccdaq.com/pdfs/anpdf/Data-AcquisitionHandbook.pdf>.
- [13] Adaptive lighting systems: Occupancy sensing, Silvair, 2020. <https://silvair.com/blog/adaptivelighting-systems-occupancy-sensing/>.
- [14] M. Wu, W. Liu, S. Zheng. Probiotic fermentation environment control under intelligent data monitoring. In *SLAS Technology*. 2024. p. 100153. Elsevier BV. <https://doi.org/10.1016/j.slst.2024.100153>.
- [15] C. K. Rao, S. K. Sahoo, F. F. Yanine. A literature review on an IoT-based intelligent smart energy management systems for PV power generation. In *Hybrid Advances*. 2024. Vol. 5, p. 100136. Elsevier BV. doi:10.1016/j.hybadv.2023.100136.
- [16] P. Neyezhmakov, S. Zub, S. Pivnenko. Preliminary e-infrastructure for digital metrology. In *Measurement: Sensors*. 2022. Vol. 23, p. 100398. Elsevier BV. doi:10.1016/j.measen.2022.100398
- [17] K. Bobrovnikova, E. Tovstukha. Methods for energy efficiency and energy saving in the smart home system. In *Computer Systems and Information Technologies*. 2020 Vol. 1, Issue 1, pp. 54–59. Khmelnytskyi National University. doi:10.31891/csit-2020-1-7.
- [18] L. Liu, Q. Peng, H. Jiang, L. Ran, Y. Wang, C. Du, J. Chen, H. Zhou, Y. Chen, Z. Peng. BP neural network for non-invasive IGBT junction temperature online detection. In *Microelectronics Reliability*. 2023. Vol. 141, p. 114882. Elsevier BV.
- [19] T. Szkopek, E. Martel. Suspended graphene electromechanical switches for energy efficient electronics. In *Progress in Quantum Electronics*. 2021. Vol. 76, p. 100315. Elsevier BV. doi:10.1016/j.pquantelec.2020.100315.
- [20] S. R. Madeti, S. N. Singh. Monitoring system for photovoltaic plants: A review. In *Renewable and Sustainable Energy Reviews*. 2017. Vol. 67, pp. 1180–1207. Elsevier BV. doi:10.1016/j.rser.2016.09.088.
- [21] P. Becker, M. F. Papa, L. Olsina. Exploratory study on the syntactic and semantic consistency of terms in project management glossaries to provide recommendations for a project management ontology. In *Science of Computer Programming*. 2024. Vol. 235, p. 103094. Elsevier BV. doi:10.1016/j.scico.2024.103094.
- [22] J. Ajayan, S. Sreejith, M. Manikandan, W.-C. Lai, S. Saha. Terahertz sensors for next generation biomedical and other industrial electronics applications: A critical review. In *Sensors and Actuators A: Physical*. 2024. Vol. 369, p. 115169. Elsevier BV.
- [23] H. Helali, A. Khedher. Performance study of control strategies applied to smart transformer model based on a five-level cascaded H-bridge rectifier. In *Computers and Electrical Engineering*. 2023. Vol. 110, p. 108864. Elsevier BV. doi:10.1016/j.compeleceng.2023.108864
- [24] T. Dubynyak, L. Dmytrotsa, M. Yavorska, N. Shostakivska, O. Manziy, *Methods and Means of Automatic Statistical Assessment of Information Measuring Systems*. ITTAP, 2023, pp. 574-585.
- [25] V. Martsenyuk, A. Sverstiuk, A. Klos-Witkowska, N. Kozodii, O. Bagriy-Zayats, I. Zubenko, Numerical analysis of results simulation of cyber-physical biosensor systems. *CEUR Workshop Proceedings*, 2019, 2516, pp. 149–164.